Computers in Biology and Medicine 108 (2019) 67–77

Contents lists available at ScienceDirect

Computers in Biology and Medicine

journal homepage: www.elsevier.com/locate/compbiomed

Directional fast-marching and multi-model strategy to extract coronary artery centerlines

Dengqiang Jia[a], Xiahai Zhuang[b,*]

[a] School of Naval Architecture, Ocean and Civil Engineering, Shanghai Jiao Tong University, Shanghai, China
[b] School of Data Science, Fudan University, Shanghai, China

ARTICLE INFO

Keywords:
Minimal path
Multi-model
Directional fast-marching
Coronary centerline

ABSTRACT

Background: Computed tomography angiography (CTA) is a non-invasive technique to image coronary arteries and evaluate coronary artery diseases (CAD). The diagnosis of CAD requires modeling anatomical structures and analyzing the function and pathology of the coronary arteries. Therefore, a robust and automated method for extracting reliable coronary artery centerlines is valuable in clinical practice.

Method: We extracted coronary centerlines using the directional fast marching (DFM) method and improved DFM with a multi-model strategy. The method comprises model guidance, the application of vessel direction, and a multi-model strategy: (1) coronary models are constructed using registration techniques and then used as prior knowledge of the vessels; (2) the vessel direction, modified from the eigenvectors of the Hessian matrix and vesselness, is used to guide the search for the vessel points during fast marching; and (3) the multi-model strategy is applied to identify suboptimal results from the overall outcome as in multi-atlas segmentation. Overlap and accuracy metrics are used to assess the segmentation. The authors evaluated the performance of the proposed method on 32 CT cardiac angiography datasets from the Rotterdam Coronary Artery Algorithm Evaluation Framework (RCAAEF). The authors also studied the effect of models on DFM.

Results: For the quantitative evaluation, DFM improved the average overlap (OV) from 43.6% of a method without model information to 77.8%. In addition, with the ground truth delineated by experts, multi-model DFM (MM-DFM) obtained 83.5% average overlap (OV) in the training datasets and 86.6% in the test datasets.

Conclusion: The authors propose a novel approach to extract coronary centerlines from CTA using DFM and further extend DFM to a multi-model strategy. DFM effectively applies the prior shape of the coronary vessels and vascular features within the target image and has the potential to achieve clinically relevant results.

1. Introduction

The American Heart Association has reported that coronary artery disease (CAD) was the underlying cause of approximately one out of seven deaths in the United States in 2014 [1]. Vascular imaging, particularly computed tomography angiography (CTA), is a non-invasive technique for diagnosing CAD [2]. In cardiovascular practice, extracting the centerline and lumen of the coronary arteries using CTA is a fundamental step in evaluating plaque extent and stenosis area [3]. Accurate extraction can lead to high-quality models for cardiovascular hemodynamics analysis, functional assessment, surgical planning, and simulation.

The methodology for centerline extraction can be classified into two groups: image-based methods and geometrical-model-based approaches.

Image-based approaches extract centerlines indirectly using image filtering and enhancing algorithms. The filters are often designed by combining widely used image processing tools, from image intensity to first- and second-order derivative edge-based detectors. Vessel-specific features such as scale, directionality, and branches are enhanced by these filters. These techniques commonly involve the Hessian matrix [4,5], the gradient vector [6,7], the structure tensor [8–10], and flux-based filters [11–13].

Geometrical-model-based methods commonly employ mathematical equations describing the geometry of the dataset to directly determine the centerline positions. These methods generally start from a set of seeds, which are also referred to as starting points, and then propagate toward the vessel of interest or the distal end of the vessel using, for example, region growing [14,15], active contours [16,17], or model matching. Model matching uses geometric models, including spheres

* Corresponding author.
E-mail address: zxh@fudan.edu.cn (X. Zhuang).

https://doi.org/10.1016/j.compbiomed.2019.03.029
Received 16 December 2018; Received in revised form 29 March 2019; Accepted 30 March 2019

[18], cylinders [19–23], and ellipsoids [24] as templates. The centerline is obtained by determining the best-fitting template at each location in the image.

The two aforementioned methods are often integrated for improved results [25]. Despite the significant progress in Refs. [5,26], centerline extraction for coronary arteries remains challenging due to the small vessel size, branch overlap, and the presence of pathology. Lessage et al. [27] provided a broad review of *vessel* extraction techniques, wherein the appearance and geometric models, image features, and extraction methods are discussed.

The minimal path is a widely used framework for centerline extraction [28–30], particularly for locating tiny vessels [31]. It can detect curve-like structures by determining the minimal-cost path between two seed points [32]. It is fast and can avoid local minima by efficiently searching for the global optima of the energy function. Several methods have been proposed to automate path propagation and relax the need for seed points in the minimal path framework. Krissian et al. [33] identified the starting point by automated aorta detection but manually annotated the endpoint for termination. Kaul et al. [34] proposed the minimal path method with key-point detection (MPWKD) to obtain a curve with a specified endpoint. MPWKD detects several key points along the curve by front propagation and terminates the procedure when the desired curve length is reached. It detects the starting point automatically but requires an appropriate stopping criterion to achieve a fully automated algorithm. Tek et al. [35] used a medialness threshold as a stopping criterion, and Kitslaar et al. [36] used the leaf points as endpoints.

To obtain a robust method for extracting coronary centerlines, Friman et al. [21] proposed a multiple hypothesis tracking (MHT) approach to segment the structure of small vessels. The authors employed a vessel template on a sphere to assess how well the geometric model fits the image data. The vessel template is generally sensitive to the homogeneous image neighborhood around tubular structures, and two manual points are required to extract the target centerlines. Kerrien et al. [23] used a RANSAC-based tracking (RBT) algorithm to extract the vessel centerline. The method is proven to outperform the MHT method on 3D neurovascular images. However, a user-defined point is required to track the entire vessel tree. To obtain more vessel features, Cetin and Unal et al. [22] estimated a high-order diffusion tensor via a flux-based model. The tensor can be used to estimate the tracking direction, which is the critical step in predicting the centerline positions. Moreover, the antipodal asymmetries in Y-junction-like vessel trees can be constructed, which is helpful for bifurcation detection. Zheng et al. [15] developed a model-driven approach to automatically extract and recognize the main branches using a learning algorithm. They used model fitting by registering a whole-heart structure model with coronary artery information to the target CTA image based on the whole-heart segmentation result [37,38]. The learning algorithm, based on the probability boosting tree and marginal space learning, provides the probability of coronary center points within a cutting plane along the coronary model. The final centerline is determined via the optimal probability path along the stacked cutting planes using dynamic programming. They employed 108 CTA volumes, with manual annotation of the coronary centerlines, to train their learning algorithm, and the method exhibited promising performance. Based on a convolutional neural network (CNN), Jelmer et al. [39] predicted the posterior probability distribution over possible tracking directions of a vessel point. The tracker then used the directions to obtain several centerline candidates by tracing from several CNN-identified seed points to the starting point. However, the automatic seed identification CNN requires training images in which all coronary arteries have been annotated, and the long centerlines are shortened to a definite length.

This study proposes using the directional information obtained from multiple coronary models and the target image to guide centerline extraction. The coronary models are constructed from the references using multi-stage, non-rigid registration methods. The directional information is integrated into the fast-marching process of the minimal path framework, referred to as directional fast-marching (DFM). DFM propagates the wavefront along the vessel, and the propagation is ensured to be consistent with the model direction. The desired propagation is achieved by introducing the concept of vessel direction, which is combined with the model direction in the DFM framework.

The proposed method is designed to manage the three typical challenges faced by the traditional minimal path framework: the leakage problem, the shortcut issue, and the seed point-and-endpoint problem [40]. First, DFM can accelerate wave propagation, particularly along the desired direction, due to the guidance of the coronary models, which has two advantages. One is that, compared with conventional methods, DFM generally has fewer visited points when the wavefront arrives at the same endpoint. The other is that the backtracked path obtained by DFM tends to avoid regions not of interest. As a result, DFM minimizes leaking and shortcut tracking. Second, DFM uses a learning-based algorithm to detect the ostia automatically, which are then used as the starting points for fast marching [41]. Finally, for termination, DFM refers to the length of the model and constructs a new stopping criterion; hence, endpoint selection is no longer required.

A preliminary method—the directional minimal path—was previously proposed in Ref. [42]. This method, referred to as $\mathrm{DMP}_{\mathrm{LL}}$ in this paper, estimates vessel vectors by connecting two points in the target image; thus, the direction is sensitive to the position of the selected points. Additionally, this estimation only enables the front to propagate along the direction that is consistent with the model direction, and it does not consider the local direction of the target vessels. This limitation is managed by DFM using the proposed vessel direction.

The remainder of the paper is organized as follows. The novel coronary centerline extraction, including a new vessel direction, DFM and the multi-model strategy, are introduced in Section 2. Section 3 describes the experiments and results. The performance and advantages of the proposed method are demonstrated. Finally, the results and future developments are discussed in Section 4.

2. Method

In this study, a new model-based method, directional fast-marching (DFM) is proposed here for coronary centerline extraction from CTA images, and it is extended to a multi-model strategy. Fig. 1 (a) and (b) show the diagram of DFM using one model and the multi-model strategy, respectively. Section 2.1 presents the basic theory of the minimal path method, where the vesselness-based fast marching (VBFM) for coronary centerline extraction is described in Section 2.1.2. Section 2.2 presents DFM methodologies for coronary centerline extraction, including model construction and several implementation details. Finally, Section 2.3 introduces our multi-model strategy for the model-guided path tracking.

2.1. Basic theory

2.1.1. Minimal path theory for path tracking

The minimal path framework minimizes the cost of a path connecting two points. The cost function is formulated using a cumulative, monotonic cost metric integrated along the path [32]. Fast-marching-based algorithms are widely used as a numerical optimization method to solve the minimization problem for low computational complexity.

Let $C \in \mathscr{A}_{p_0,p_1}$ refer to a curve connecting two points p_0 and p_1, and $\mathscr{A}_{p_0,p_1}$ be the space of all these curves. The energy for a curve C is denoted by $E(C)$ and consists of two parts. One is the integration of the potential along the curve, referred to as $P(C)$, and the other is related to the arc length of C, that is, $L(C)$. Therefore, the energy is defined as follows:

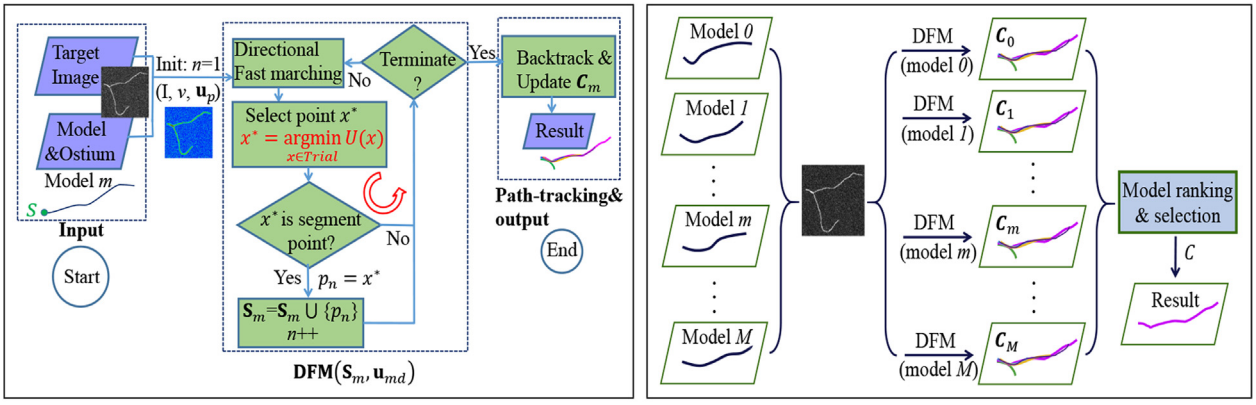

Fig. 1. Diagram of the single-model DFM for centerline extraction (a) and the multi-model strategy (b).

$$E(C) = \omega L(C) + (1-\omega)\int_{s\in[0,L]} P(C(s))ds = \int_{s\in[0,L]} \tilde{P}(C(s))ds, \tag{1}$$

where $\tilde{P} = \omega + (1-\omega)P(C(s))$, and $C(s) = p_s$ is a point on the curve C parameterized by the arc length $s \in [0, L]$.

Let U be the surface of minimal action that starts at p_0. Therefore, $U(p)$ is defined as the greatest lower bound of the energy, which corresponds to the minimal energy integrated along a path that starts at p_0 and ends at p, that is,

$$U(p) = \inf_{C\in\mathscr{A}_{p_0,p}} E(C) = \inf_{C(L)=p} \int_C \tilde{P}ds, \tag{2}$$

which can be calculated by solving the Eikonal equation:

$$\begin{cases} \|\nabla U(p)\| = \tilde{P}, \text{ for } p\in\Omega \\ U(p_0) = 0. \end{cases} \tag{3}$$

Fast marching can solve the Eikonal equation efficiently. The method computes $U(p)$ while visiting the grid points in an increasing order using Dijkstra's algorithm. In this framework, every grid point is marked and classified into three classes: (1) alive points, for which U has been computed and frozen; (2) trial points, for which U has been computed but not frozen; and (3) far points, for which U is yet unknown. The trial points form the interface of the wave (wavefront) between the far and alive points, and trial points with the smallest U value in each iteration are selected as alive points.

After the Eikonal equation is solved, the U values in an image are calculated, and a minimal energy path from any current point to the starting point can be generated using the backtracking scheme [34].

2.1.2. Vesselness-based fast-marching

Multi-scale vesselness filters are usually applied before segmentation and visualization, which enhance the tube structure of the image and facilitates the extraction of curve skeletons [25,43]. Vesselness is defined using the eigenvalues of the Hessian matrix of the image.

Let $\mathscr{H}_{x,\sigma}$ be the Hessian matrix at a point x computed at scale σ, and $\lambda_{\sigma,k}$ denote the k^{th} (k = 1, 2, 3 in the 3D case) eigenvalue in ascending order, whose corresponding normalized eigenvector is $\mathbf{u}_{\sigma,k}$; $\mathscr{H}_{x,\sigma}\mathbf{u}_{\sigma,k} = \lambda_{\sigma,k}\mathbf{u}_{\sigma,k}$. The vesselness at scale σ is defined as follows:

$$v_o(x,\sigma) \triangleq \begin{cases} 0, & \text{if } \lambda_{\sigma,2} > 0 \text{ or } \lambda_{\sigma,3} > 0 \\ \left(1 - e^{-\frac{\mathscr{R}_A^2}{2a^2}}\right) e^{-\frac{\mathscr{R}_B^2}{2b^2}} \left(1 - e^{-\frac{\mathscr{R}_S^2}{2c^2}}\right), & \text{otherwise} \end{cases}, \tag{4}$$

where $\mathscr{R}_A \triangleq |\frac{\lambda_{\sigma,2}}{\lambda_{\sigma,3}}|$, $\mathscr{R}_B \triangleq \frac{|\lambda_{\sigma,1}|}{\sqrt{|\lambda_{\sigma,2}\lambda_{\sigma,3}|}}$, and $\mathscr{R}_S \triangleq \sqrt{\sum_{j=1}^{3}\lambda_{\sigma,j}^2}$. The parameters a, b, and c tune the sensitivity of the filters to deviations in $\mathscr{R}_A$, $\mathscr{R}_B$, and $\mathscr{R}_S$, respectively.

The vesselness function is defined using multi-scale filters as follows:

$$v(x) = \max_{\sigma_{min}\le\sigma\le\sigma_{max}} v_o(x,\sigma). \tag{5}$$

In the experiments, the minimum scale was set to $\sigma_{min} = 0.5$ mm, the maximum scale to $\sigma_{max} = 3$ mm, and the step size to 0.2 mm, which correspond to the radius range of the coronary arteries. Fig. 2 (a) and (b) show an example of a 2D image and its corresponding vesselness feature image.

Based on the definition of vesselness in (5), the local principal vector $\mathbf{u}_p$, which will be later used for the definition of the vessel vector, is defined as follows:

$$\mathbf{u}_p(x) = \mathbf{u}_{\sigma_p,1}(x), \tag{6}$$

where $\sigma_p = \underset{\sigma_{min}\le\sigma\le\sigma_{max}}{\text{argmax}}\ v_o(x,\sigma)$. Fig. 2 (b)-(e) illustrate the $\mathbf{u}_p$ vector using the vector field in 2D cases.

Vesselness-based fast-marching (VBFM) adopts the following

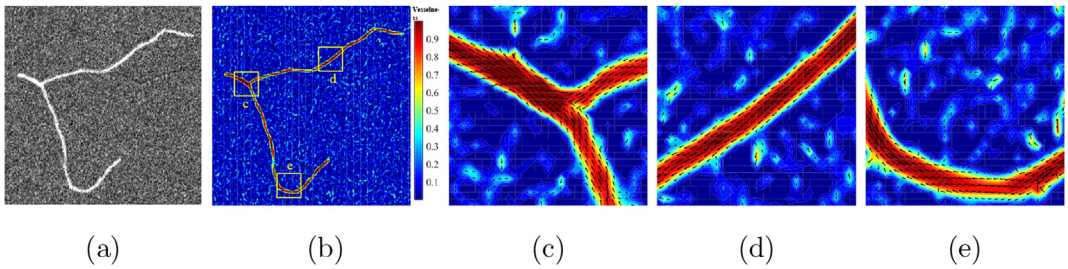

Fig. 2. Illustration of the vesselness feature and the principal direction information in DFM. (a) The original synthetic 2D image containing a region with a higher mean intensity value than that of the random background. (b) Illustration of the principal directions (black arrows) and normalized vesselness magnitude (ranging from 0 to 1) using the vector field. (c)–(e) Close-up images of the three positions in (b).

potential function that incorporates vesselness:

$$P_v(x) = \frac{1}{v(x)^{\alpha} \cdot s(x)^{\beta} + \varepsilon}, \tag{7}$$

where $v(x)$ and $s(x)$ denote the vesselness term and the intensity similarity term, respectively, α and β are parameters controlling the contrast between these two terms, and ε is a small positive value to prevent singularities. The similarity term can be defined as follows [30]:

$$s(x) = \begin{cases} e^{-\frac{1}{2}\left(\frac{I(x)-\mu_{ca}}{\sigma_{ca}}\right)^2}, & I < \mu_{ca}, \\ 1, & I \geq \mu_{ca} \end{cases} \tag{8}$$

where $I(x)$ is the intensity at the point x, and μ_{ca} and σ_{ca} are the intensity mean and the standard deviation of the coronary lumen, respectively.

2.2. Model-guided directional fast-marching

VBFM is an image-based method that favors visiting the vessel-like region in the target image during fast marching. However, it is sensitive to the starting points' locations; moreover, it requires an appropriate stopping criterion. Here, DFM is proposed to combine the real vessel and the model directions for fast marching.

DFM is guided by models that incorporate prior information for centerline extraction. Its pipeline diagram is shown in Fig. 1(a). DFM is initialized with model construction (Section 2.2.1) and starting point (ostium) detection. After iterations of directional fast marching, a set of segment points is obtained. Consequently, a set of paths can be traced by backtracking from the segment points to the starting point, and the final target centerline is obtained from the curve set. The stopping criterion is designed by incorporating the information from the coronary model. The implementation details are elaborated in Section 2.2.3.

2.2.1. Model construction

The term *model* in this study refers to a pre-constructed centerline containing geometric information (for example, the shape and length) of the vessel under study. Models of coronary centerlines are referred to as coronary models.

The model is constructed via the following steps: a CTA volume is first selected from the training set as the common space. Subsequently, the remaining training images are registered to the selected common space using a multi-stage non-rigid registration algorithm (MSR) [44]. The resulting transformations are then used to map the regularly-spaced points of the corresponding centerlines of the CTA images to the common space. The transformed points are finally fused to create a centerline, which is the resulting coronary model. The fusing process is based on the one-way distance algorithm (OWD) proposed by Zheng et al. [15]. The unique common space is a CTA image selected from one of the training CTA datasets. A different model can be constructed using another CTA and the corresponding training centerlines. The resulting model generally has a length similar to the maximal length among all of the training centerlines. In the experiment, the average length of the constructed models is 10–20% larger than the mean length of all of the centerlines from clinical datasets.

When the coronary model is used for centerline extraction from a target CTA image, it should be mapped to the target CTA using an image registration process for initialization and guidance. A model contains one centerline for extracting one branch. If two branches are to be extracted, two corresponding models are required, and two DFM processes should be applied separately.

2.2.2. Directional fast-marching

In DFM, the potential function $P_v(x)$ is defined in (7). It incorporates the vessel direction as follows:

$$P_d(x) = \frac{1}{v(x)^{\alpha} \cdot s(x)^{\beta} \cdot d(x)^{\delta} + \varepsilon}. \tag{9}$$

In the experiments, the parameters α, β, and δ were set to 1, 1, and 2, respectively; the direction term $d(x)$, which is a decay function, indicates the cost from the model and vessel directions:

$$d(x) = e^{-(G(x)-1)^2}, \text{ and}$$
$$G(x) = \frac{\mathbf{u}_{vd}(x) \cdot \mathbf{u}_{md}(x)}{|\mathbf{u}_{vd}(x)| \cdot |\mathbf{u}_{md}(x)|}, \tag{10}$$

where $\mathbf{u}_{vd}(x)$ is the *vessel vector* along the vessel direction at point x, and $\mathbf{u}_{md}$ is the *model vector* (described in Section 2.2.3) providing the prior direction information of the model.

The *vessel vector* $\mathbf{u}_{vd}(x)$ is computed from the principal vector as follows:

$$\mathbf{u}_{vd}(x) = \text{sign}(\overrightarrow{p_{n-1}x} \cdot \mathbf{u}_p(x))\mathbf{u}_p(x), \tag{11}$$

where p_{n-1} is the segment point (defined in Section 2.2.3), and x is the current visiting point. The local principal vector $\mathbf{u}_p(x)$ in (6) is not directly used, as the front may propagate in either of the directions $\mathbf{u}_p(x)$ and $-\mathbf{u}_p(x)$. Using $\text{sign}(\overrightarrow{p_{n-1}x} \cdot \mathbf{u}_p(x))$ ensures that the wave propagates along the current direction from the previous to the current visiting point, consistent with the direction from the distal part to the proximal part of the coronary branch. This can be achieved using the combined

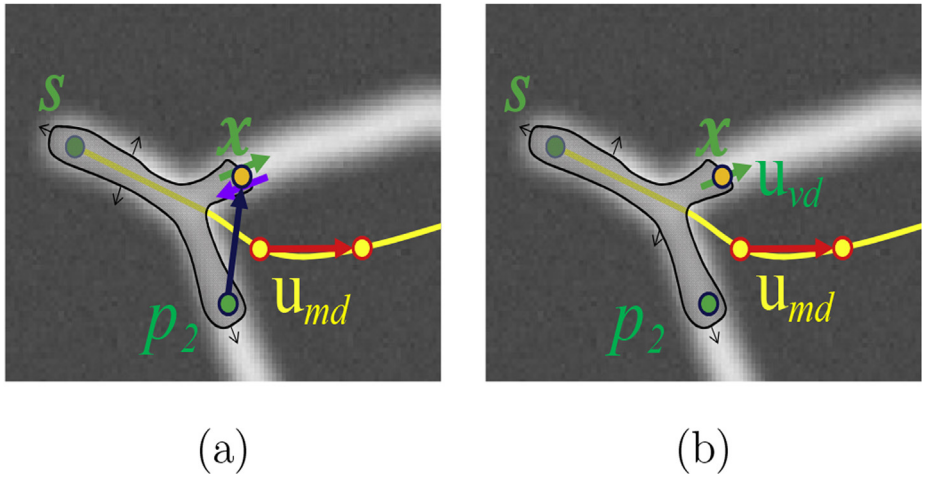

Fig. 3. Illustration of the direction information. (a) The two opposite directions along the vessel principal vector at x. (b) The vessel vector, $\mathbf{u}_{vd}(x)$, selected at x. S is the starting point, p_2 is the segment point, and $\mathbf{u}_{md}(x)$ is the model vector.

information from the segment point and the current visiting point, as shown in Fig. 3 (a) and (b). Using the vessel vector $\mathbf{u}_{vd}(x)$, the DFM wavefront propagates faster in the region containing points along the desired direction.

2.2.3. Implementation details

The framework of the proposed DFM is shown in Fig. 1(a). In this section, the implementation details of DFM are explained from three perspectives.

2.2.3.1. Ostium detection. For ostium detection, the coronary model is first registered to the target image, which provides the initial locations of the two coronary ostia. The ostia are then accurately detected via a learning-based algorithm [15,41]. In the multi-model strategy, multiple models initialize and then detect one ostium, thus returning multiple results. Subsequently, they are fused by computing their mean to provide the final ostium detection result. The left and right ostia are used as the starting points for DFM in extracting the left and right branches, respectively.

2.2.3.2. Path tracing. The direction information of the model guides the propagation of the front line in DFM. This information is referred to as the model direction. However, compared to one iteration step in the front propagation, the computation of this model direction is time consuming. Therefore, it is proposed to divide the front propagation procedure into N stages. At the beginning of each stage, the model direction is extracted and computed, and then remains constant. This method avoids updating the model direction in each iteration of the front propagation; hence, it is computationally efficient. The model direction, indicated by the *model vector*, is computed using two selected model points.

The *model points* refer to all of the points obtained by equidistantly resampling the model centerline. The starting point of the model vector is the model point whose position is closest to the segment point, which is detected in the previous stage. The endpoint is another model point determined according to the combination of the curvature of the model centerline and the length constraint. *The segment points* are located on the path of the target coronary artery during front propagation. They are the key points for obtaining the target centerline. The trial point with the minimal action value (U in Equation (2)) is considered a candidate segment point (x^* in Fig. 1(a)) at each step of the front propagation. A candidate is selected as a segment point, that is, $p_n = x^*$, if the following two conditions are satisfied:

(1) The distance between the previous segment point and the candidate point is not less than the magnitude of the model vector, that is, $\| \overrightarrow{p_{n-1}x^*} \| \geq \|\mathbf{u}_{md}\|$.
(2) The angle θ between the vessel vector and the model vector is not larger than 30°, that is, $\theta \in [0,30]$.

The DFM procedure for obtaining the n^{th} segment point using model m is referred to as DFM($\mathbf{S}_m$, $\mathbf{u}_{md}$), where $\mathbf{S}_m$ denotes the set of segment points and $\mathbf{u}_{md}$ is the model vector in the n^{th} stage. Fig. 1 (a) shows the iterations for detecting the segment points.

2.2.3.3. Stopping criteria. The resulting centerlines of the minimal path can be obtained by backtracking from each segment point in $\mathbf{S}_m$ to the original starting point S. Once the stopping criterion for terminating the fast-marching process is met, several backtracked centerlines are then added to the curve set $\mathbf{C}_m$, which contains the centerline extraction results directed by model m. The stopping criterion is satisfied if the following conditions are met:

(a) The segment point detection has reached a maximum number of stages.
(b) The fast-marching process has visited a maximum number of points.
(c) The curve obtained by backtracking is longer than the coronary model.

Because the length of the model is used as a stopping condition for backtracking, the model that was applied is an extended mean centerline to ensure that it is sufficiently long. The effects of model length are studied in Section 3.7.3.

2.3. Multi-model strategy

As shown in Fig. 1 (a), the single-model DFM uses a coronary model combined with the starting point to extract centerlines from a target image. The multi-model strategy uses more than one model to compensate for the potential bias associated with one particular model. This multi-model strategy resembles the multi-atlas scheme that has been well developed in atlas-based segmentation [45]. Multi-atlas segmentation applies multiple atlases to segment a target image, resulting in multiple segmentation results. These results are then fused in a multi-classifier framework to generate a final single segmentation. Fig. 1 (b) illustrates the multi-model strategy for centerline extraction.

With the curve sets $\mathbf{C} = \cup_{m=0,1,2,\ldots,M}\mathbf{C}_m$ obtained by DFM, where M is the number of models, the final result C can be generated from $\mathbf{C}$. Generally, the maximal length is a useful criterion for model ranking and selection. However, in the experiments, the reference points provided by the Challenge organizers were used to select a target branch for evaluation. Section 3.5 provides details.

3. Results

3.1. Materials

The RCAAEF provides 32 publicly available cardiac CTA images and standardized measurements assessing the performance of different algorithms [2]. The dataset consists of 8 training cases and 24 test images, with a voxel size of approximately $0.32 \times 0.32 \times 0.4$ mm. The gold standard for the vessels in each image is selected for annotation by the RCAAEF organizers, yielding 128 vessels. Only the centerlines of the training datasets are available to the participants.

3.2. Evaluation metrics

The RCAAEF provides four standardized measurements to evaluate centerline extraction capability and accuracy [2], namely, overlap (OV), overlap until the first error (OF), overlap with the clinically relevant part of the vessel (OT), and average inside (AI). OV represents the ability to track the complete vessel and ranges from 0 (implying no overlap between the reference and the target) to 1 (indicating a perfect overlap). OF determines the portion of the coronary centerline that has been extracted before the first error. It ranges from 0 to 1. OT indicates how well the method can track the centerline that is assumed to be clinically relevant, and ranges from 0 to 1, with 0 in the worst case and 1 in the best case. AI is the average distance between two centerlines and represents the accuracy of the centerline extraction if the evaluated centerline is inside the vessel.

To evaluate the similarity of two centerlines, the target and reference centerlines are resampled into a set of equidistributed points. The points on the target, which are within a preset distance to the reference centerline, are labeled as true-positive points of the target (TPT). The remaining target points are regarded as false-positive points (FP). Further, the RCAAEF considers the sample points in the reference that are within a preset distance to the target centerline to be true-positive points of the reference (TPR). The remaining points of the reference are regarded as false negative (FN). Then OV is defined as follows:

Table 1
Parameter setting for DFM. Parameter setting for DFMParameter setting for DFM.

Items	Parameters	Recommended values
P_{tl} in (9)	$\{\alpha, \beta, \delta\}$	{1,1,2}
$v_o(x, \sigma)$ in (4) and $v(x)$ in (5)	σ	3*D*: [0.5, 3], *step* = 0.2 2*D*: [0.5, 2.5], *step* = 0.1
	$\{a, b, c\}$	{0.5, 0.5, 100}
Segment point conditions	θ	[0, 30°]
Stopping criterion	Maximum number of stages	30
	Maximum number of points	2,000, 000

$$OV = \frac{||\mathrm{TPT}_{ov}|| + ||\mathrm{TPR}_{ov}||}{||\mathrm{TPT}_{ov}|| + ||\mathrm{TPR}_{ov}|| + ||\mathrm{FN}_{ov}|| + ||\mathrm{FP}_{ov}||}.$$

3.3. Parameter setting and study

Table 1 summarizes the four parameters groups in DFM. The three parameters α, β, and δ in the potential function (9) control the balance of the vesselness, intensity similarity, and direction terms, respectively. They are generally set as $\alpha = 1$, $\beta = 1$, and $\delta = 2$. To study their effect, an experiment was conducted by fixing one parameter and letting the other two vary. Fig. 4 shows the distribution of the OV values concerning the two parameters.

3.4. Single-model DFM (SM-DFM)

Fig. 5 shows the box plots of SM-DFM extraction using real coronary models. Here, the real model refers to the model constructed using the training data. The average OV values for the three branches obtained by SM-DFM using the real models were as follows: 89.8% ± 7% (RCA), 68.8% ± 25% (LAD), and 74.6% ± 23% (LCX). Further, SM-DFM produced evidently better OV results than the previous single-model $\mathrm{DMP}_{\mathrm{LL}}$ (SM-$\mathrm{DMP}_{\mathrm{LL}}$ [42]), namely, 77.8% VS 57.7%, with statistical significance ($p < 0.001$), because the vessel direction was used.

The SM-DFM extraction results for two cases (LAD from datasets 03 and 07) were particularly weaker than the others. The red diamonds in the green rectangle in Fig. 5 demonstrate that all of the OV metrics for LAD from these two datasets were less than 50% using any of the seven real models.

3.5. Multi-model DFM (MM-DFM)

The effect of the multi-model strategy is studied in this section. Each training dataset was considered a target dataset, and the remaining were used as models. Three major coronary branches were extracted by detecting the candidate segment points, resulting in 24 target centerlines for multi-model-based extraction. Fig. 7 shows an example. DFM detected numbers of segment points using multiple models, and three resultant centerlines were selected using the multi-model strategy.

Table 2 demonstrates that MM-DFM performed significantly better than SM-DFM in all of the evaluation metrics. Notably, for example, MM-DFM improved the OV score of SM-DFM from 77.8% to 83.5% ($p < 0.001$).

Fig. 6 shows that the proposed model selection method may choose suboptimal branches from the resulting centerline set. Additionally, the blue boxes indicate two branches at which SM-DFM performed poorly using all of the available models.

3.6. Results from the RCAAEF competition

To compare MM-DFM with other state-of-the-art methods, we participated in the RCAAEF competition. The three main branches were extracted from the 24 test images and were sent to the RCAAEF organizers for evaluation. The evaluation was blind to the participants.

Table 3 presents the evaluation results. The three average overlap metrics, namely, OV, OF, and OT, for the proposed method were 86.6%, 49.1%, and 89.1%, respectively. The average accuracy metric, referred to as AI, for the proposed method was 0.49 mm.

Table 4 presents the comparison between the proposed method and other nine automatic methods published by the RCAAEF. MM-DFM ranked sixth based on the OV metric.

The model selection algorithm also has a significant impact on performance. Fig. 8 provides an example for illustration. The model and target vessel in this example exhibit different directions toward the distal end. Thus, DFM fails to extract the full length of the target centerline. As shown in Fig. 8, the resulting centerline (blue) is shorter than the target vessel (as indicated by the red arrows). The effect of the models on the performance of DFM will be studied in the following section.

3.7. Effect of models on DFM

Three experiments were conducted to evaluate the impact of the models on DFM. A fast-marching method based on vessel direction without model guidance, referred to as VDOFM, was first examined. Subsequently, real models from the RCAAEF training datasets and simulated models were used to assess the performance of SM-DFM. Finally, a model length study was conducted using models of different lengths.

3.7.1. SM-DFM versus VDOFM

As VDOFM does not use any model information, the front propagation stops when the maximum number of visited points is reached, or the fast marching reaches a manually selected endpoint. Table 2 shows the quantitative results of VDOFM. SM-DFM exhibits evidently better OV than VDOFM, 77.8% VS 43.6%, with statistical significance ($p < 0.001$) due to the direction information from the models.

3.7.2. SM-DFM using real and simulated models

Real models were used to simulate a large set of models for experiments, and deformed model centerlines were created by assigning random displacements to five control points. The control points were

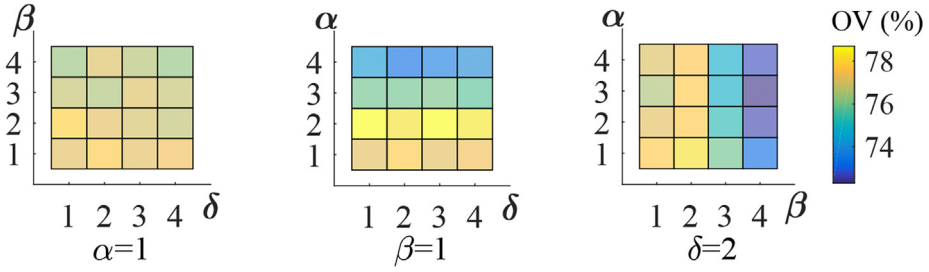

Fig. 4. OV variations with respect to α, β, and δ using DFM.

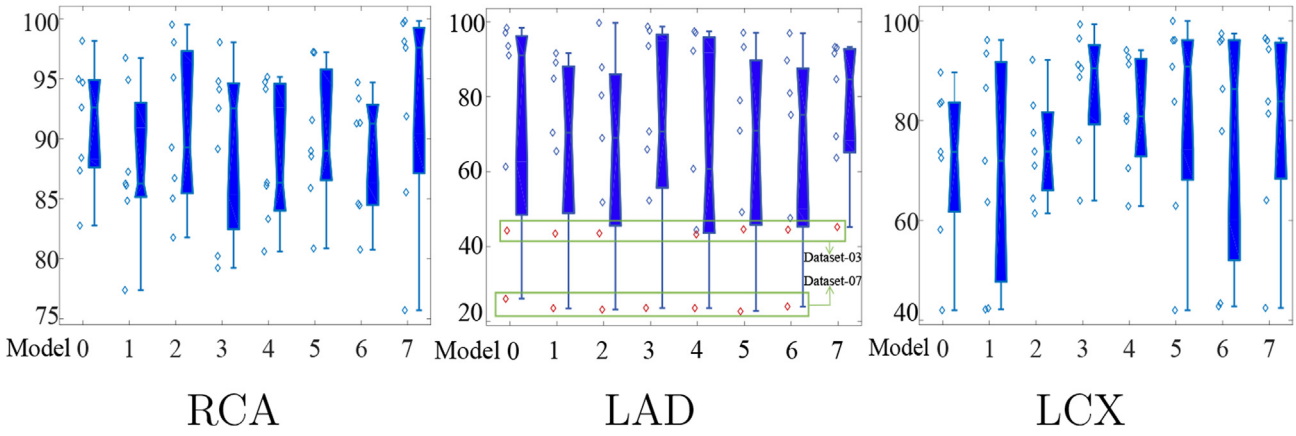

Fig. 5. Illustration of extracting different datasets using varying models. Three main coronary branches are extracted via the single-model DFM, using eight real models (indexed from 0 to 7). The results are presented as the overlap (OV) metric. The red diamonds in the green boxes indicate the results of LAD from datasets 03 and 07. Please refer to the text for more details.

model points equidistributed on the real models, and the displacements ranged from 2 to 15 mm on the normal plane to the real model centerlines. The simulated models were then obtained following a curve-fitting process to the offset control points.

Fig. 9 shows the OV results of SM-DFM using the simulated models. In this case, SM-DFM obtained an average OV of 76.4% ± 20%, compared to 77.8% ± 19% from the SM-DFM using the real models. The p-value between the two methods was 0.061, indicating no significant difference between the two groups of results.

3.7.3. Model length study

Ten model sets were simulated by truncating the real coronary models into models with different proportions (P) with respect to the full length. The value of P ranged from 10% to 100%. Subsequently, each model set was used to extract the three main vessel centerlines of the training datasets. This resulted in 168 cases, 3 (branch) × 7 (model) × 8 (image), for each model set. Fig. 10 shows the results. The performance of centerline extraction by SM-DFM, indicated by the average OV, improves with model length, and stabilizes after P = 70%.

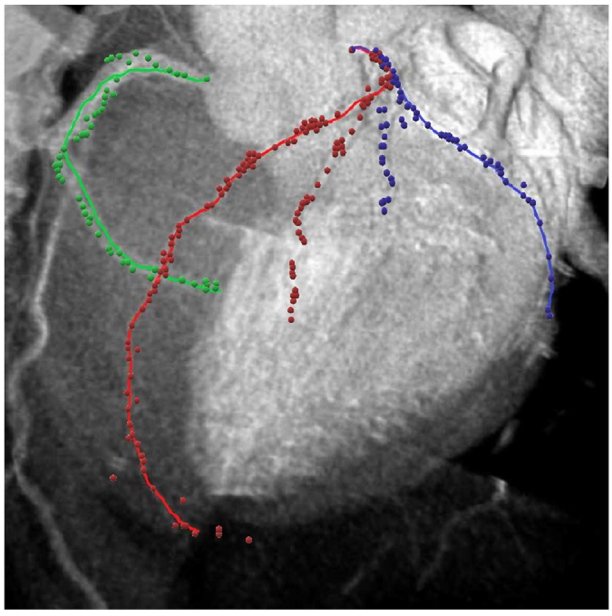

Fig. 7. All of the detected segment points and the resultant centerlines obtained via multi-model DFM: RCA (green), LAD (red), and LCX (blue).

4. Discussion

The capability of a new model-based minimal path framework, DFM, to extract the coronary centerlines from cardiac CTA was explored. The method comprises model guidance, the application of vessel direction, and a multi-model strategy.

The model, which incorporates prior vessel information, facilitates

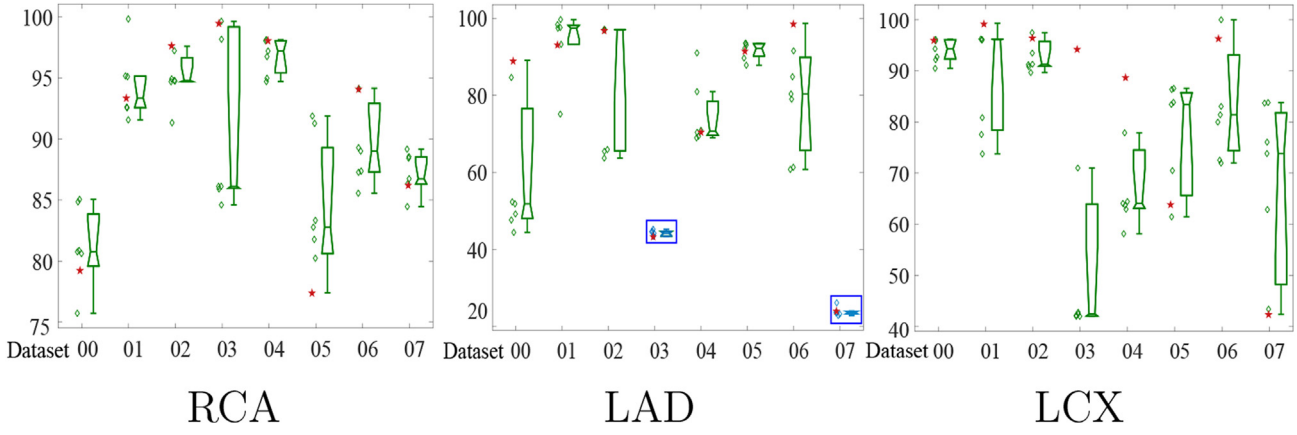

Fig. 6. Illustration of each dataset extracted via different models. The red stars indicate the centerlines selected by an automatic model selection method. The boxplots in the blue box are the results of LAD from datasets 03 and 07.

Table 2
Standardized scores of the coronary artery extraction using the fast-marching method based on vessel direction without model guidance (VDOFM), single-model DMP_{LL} (SM-DMP_{LL}), single-model DFM (SM-DFM), and multi-model DFM (MM-DFM) on the RCAAEF training datasets.

	OV (%)	OV score	OF (%)	OF score	OT (%)	OT score	AI (mm)	AI score
VDOFM	43.6	22.7	26.6	17.2	44.1	22.4	0.68	27.0
SM-DMP_{LL}	57.7	30.4	30.5	18.7	65.3	32.8	0.70	20.9
SM-DFM	77.8	44.1	51.2	30.7	80.5	47.7	0.51	28.1
MM-DFM	83.5	51.0	57.8	44.2	87.1	59.1	0.48	28.6

Table 3
RCAAEF scores of the coronary artery extraction using the proposed multi-model DFM (MM-DFM) on the test datasets.

Measure	Measurement			Score			Rank		
	Min.	Max.	Avg.	Min.	Max.	Avg.	Min.	Max.	Avg.
OV	10.3%	100%	86.6%	5.2	100	49.1	1	25	16.0
OF	2.9%	100%	49.1%	1.7	100	32.0	1	25	16.4
OT	11.1%	100%	89.1%	5.6	100	53.9	1	25	14.4
AI	0.28 mm	1.41 mm	0.49 mm	10.7	55.3	26.0	12	25	19.6
Total	–	–	–	–	–	–	8	24.8	17.6

Table 4
Results of 10 automatic methods as evaluated by the RCAAEF. Three main branches of the coronary centerlines are selected for the evaluation.

Measure	OV (%)	OF (%)	OT (%)	AI (mm)
Model Driven Centerline [15]	93.8	75.5	95.4	0.20
GFV Coronary Extractor [5]	93.3	73.7	95.7	0.29
GVFTube'n' Linkage [6]	93.0	73.8	95.7	0.35
Supervised Extraction [46]	90.3	71.5	92.3	0.24
COR Analyzer[a]	87.4	72.4	89.6	0.24
Our method	**86.6**	**49.1**	**89.1**	**0.49**
Depth First Model Fit [47]	84.4	63.6	86.7	0.28
Auto Coronary Tree [35]	84.1	58.6	85.7	0.32
CocomoBeach [36]	77.9	63.3	80.0	0.30
Virtual Contrast [52]	77.2	55.9	80.1	0.37

[a] http://www.rcadia.com/.

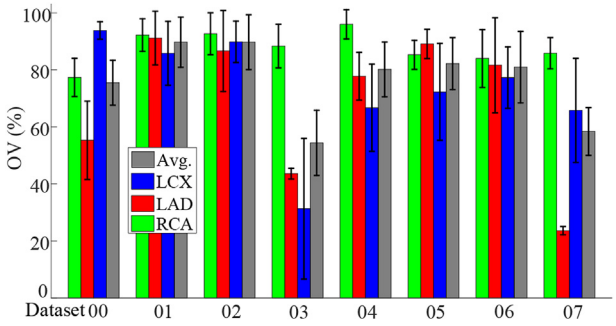

Fig. 9. The mean and standard deviation of the overlap (OV) values obtained by the single-model DFM (SM-DFM) using the simulated models.

the search for points in the desired direction. In contrast, in the absence of model information, more non-vessel points should be visited to meet the stopping criteria. Table 2 shows that the method without model direction obtained an average OV score of 43.6%, significantly worse than that obtained by the two DFM-based methods ($p < 0.001$). This is because in the fast marching process, more non-vessel points with similar minimal action values to those in the vessel region, for example, points in neighboring structures and noise, are prioritized. Hence, if the model is absent, these points tend to be false segment points, which may lead to wrong centerlines.

The model has an impact on the performance of DFM due to its shape and length. Several approaches have been proposed to train a shape model by detecting several candidate points (seeds) and then optimize it using a fitting method [46,47]. Although the shape model improves the overlap scores, most failures occurred in complex cases,

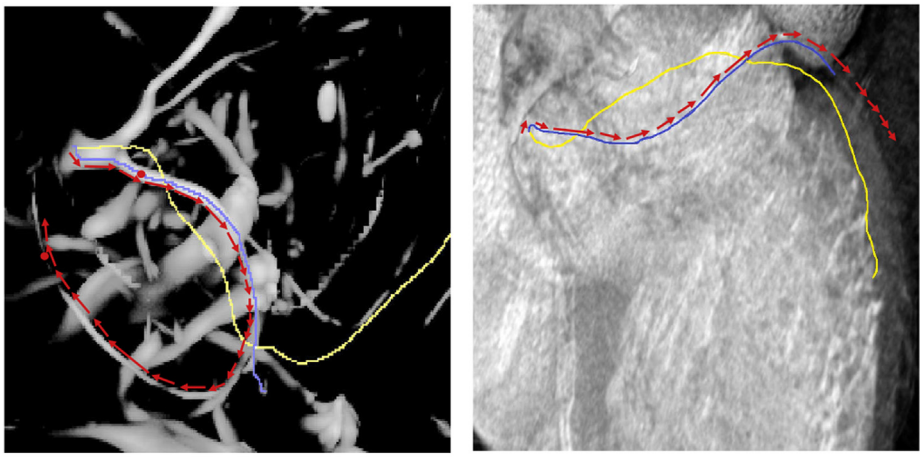

Fig. 8. An example displayed in two views showing that the shape of the model affects the performance of DFM. (a) The coronary model (yellow) and the resultant centerline (blue) of DFM using the maximal intensity projection (MIP) of the 3D vesselness image. (b) The resultant centerline (blue) and coronary model (yellow) on 3D CTA image using volume rendering. The red points in (a) are the two reference points provided by the RCAAEF. The red arrows represent the direction of the target vessel.

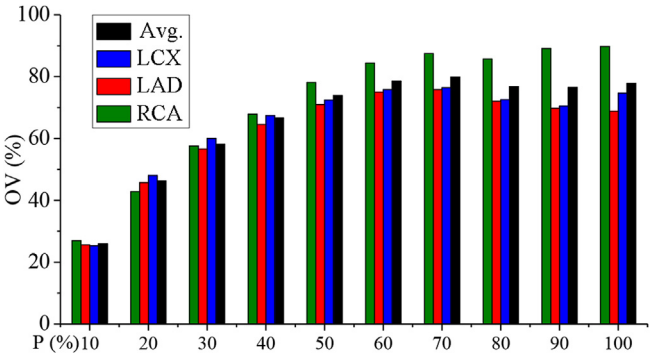

Fig. 10. Effects of the model length on the performance of SM-DFM. Ten groups of models are used with different lengths, ranging from 10% to 100% with respect to the full length of the original real models. The OV results are displayed for the three main branches and their average values.

such as unclear image contrast near the distal part of the branches. In this study, no significant difference was observed between the results obtained using real models and simulated models ($p = 0.061$). In addition, the performance of DFM improves with model length and stabilizes when $P > 70\%$ (Fig. 10). This is because the average length of the real models is larger than that of the target centerlines: the average length of the models is 169 mm, and that of the target centerlines is 145 mm. Therefore, to extract the full length of the target vessel centerlines, the model for SM-DFM should be longer than the target. Fig. 10 demonstrates that the OV values of LAD decrease when the length percentage exceeds 70%. This is because the LAD models are generally longer than the target LAD and always have apex wrapping [48,49]. When these constructed LAD models are used to guide the extraction of a target LAD that does not wrap the apex, the result could be poor, and thus the geometrical information of the models should be explored.

In addition to the model, some high-level features such as vessel direction and spatial locations are embedded into the fast marching. The vessel direction, representing a critical vascular feature, facilitates the search for points of the target image. Combining vessel and model directions ensures that the wavefront will propagate along the regions of interest, that is, the vessel lumen. Table 2 demonstrates that DFM performs better than DMP_{LL} in the single-model strategy. This is because the vessel direction, which is modified by the vessel features (vesselness) instead of an estimated vector, improves segment point detection and centerline candidate extraction. This can minimize the possibility of the front propagation stepping into non-vessel areas (leakage problem), and prevents the fast marching from being stuck in some local regions. Vessel spatial locations are detected by the enhancement filters. Several techniques have been described to improve the enhancement performance. In Refs. [5,6], a discriminator based on local geometric features was used to decrease the false positive responses. A multi-scale medialness filter [35] and a ray-casting filter [47] have been developed for better performance. The traditional vesselness filter was used in this study. Figs. 5 and 6 show that the LAD results from datasets 03 and 07 were particularly poor compared to those from the others. This is because the challenges from the images and the vessel enhancement may limit the performance of the method, even if vessel information from different coronary models is available. The image quality of dataset 03 was visually assessed as poor, and the calcium score of dataset 07 was assessed as severe, as per the description of the datasets provided by the Challenge organization (http://coronary.bigr.nl/centerlines/index.php). According to the requirements mentioned in Ref. [50], an effective vessel enhancement filter should be explored.

The centerlines are obtained via a path tracing technique using the segment points and the model points. The segment points provide two critical functions for automated centerline extraction. One is that no user-input endpoint is required to terminate the wave propagation. The other is that the set of segment points can be used to backtrack a set of minimal paths that can be combined to generate the desired centerline.

A multi-model strategy was proposed and incorporated into DFM to further improve the performance by enriching the set of segment points and candidate centerlines. Fig. 7 shows that DFM can detect segment points around not only three main branches, but also the nearby branches, due to the vessel features and the coarse directions provided by multiple models. Thus, the average OV was significantly improved from 77.8% (single model) to 83.5% ($p < 0.001$).

4.1. Runtime of the framework

All of the segmentations were performed on an Intel Core i5-6200U CPU @ 2.30 GHz computer with 4 GB system memory. The runtime of the proposed framework is related to the model construction, vesselness calculation, ostium detection, DFM extraction and multi-model strategy. It takes less than 2 s to select a centerline using multi-model strategy or detect an ostium of the target image. The model construction compromises multi-stage registration (MSR) [44] and one-way distance approach (OWD) [15], which take 10.2 min per image pair and 1 s per model on average, respectively. We applied the multi-scale vesselness filter [25] to the target CT image, which takes 8.5 min per image. Moreover, the average runtime of DFM to extract a branch from the target image using a model is 3.4 min.

Parallel computation, such as GPU programming, is an effective strategy to reduce the runtime of registration [44]. Reducing the number of points and selecting the appropriate scales are potential ways to improve the vesselness computing efficiency. Moreover, the calculation time of DFM depends on the update of the minimal action values of the wavefront and the parameters of the stopping criterion. Adopting an efficient method with good stopping criteria, without affecting the accuracy, is another useful strategy to accelerate DFM extraction.

4.2. Limitations and future work

The limitations of this study are primarily related to the insufficient investigation of vesselness filters and the limited number and quality of the coronary models. For example, as shown in Table 4, the proposed method ranked sixth in terms of the OV metric on the test datasets. Among the other methods, Zheng et al. [15] achieved an average OV of 93.8%, which is the best result. They used 108 vol of external training images. In contrast, the proposed method used only eight training datasets as models. As in multi-atlas segmentation [51], the number of available models determines the potential optimal performance of multi-model approaches. The OF metrics (in Tables 2 and 3) obtained by MM-DFM is still low (57.8% in the training datasets and 49.1% in the test datasets). This is primarily because the vessel feature enhancement is sensitive to the intensity non-uniformities of images, the presence of calcium, and pathologies [50]. This limitation could lead to erroneous centerline extraction at the proximal areas of the coronary arteries, as in the poor LAD centerline extraction results for datasets 03 and 07. The AI values in Tables 2 and 3 obtained using the proposed method are low (0.48 mm in the training datasets and 0.49 mm in the test datasets), because DFM simply pursues higher OV scores that indicate more complete vessels instead of adjusting the results to the accurate center positions. Refinement techniques of the centerlines obtained by DFM will be explored in the subsequent work.

In addition to exploring an effective vessel enhancement filter, there are three potential directions for future work on the coronary model. First, the method used to construct the coronary models could be further investigated. In this study, non-rigid registration was used to align the training centerlines into a common space and then construct the models for only three main branches using a fusion algorithm. However, different registration and fusion methods could be explored,

and models for more branches should be constructed. Second, the proposed method was tested using RCAAEF data, and for fairness, only eight training datasets were available for constructing the coronary models. In contrast, a significantly larger number of models is used in multi-atlas segmentation. As the number of models determines the potential performance of DFM, more models should be constructed and used for further studies. Finally, in this study, a simple model selection and fusion algorithm were used, that is, selecting one centerline from the set of candidates. In the future, algorithms that can select and fuse multiple resulting centerlines should be explored.

5. Conclusion

This study proposed a novel method for the fully automated extraction of coronary centerlines, one of the most challenging tasks in coronary image analysis. This method combines the real vessel and model directions into the minimal path framework. It ensures that the wave will propagate along the desired direction and prevents leakage and shortcut problems. A point set containing the segment points is constructed, and the resultant centerlines are obtained. Furthermore, the multi-model strategy, resembling the well-developed multi-atlas strategy in the image segmentation field, is developed, and further applied to improve the performance of coronary centerline extraction. The proposed method has been tested using the RCAAEF. The method obtained an average OV of 86.6%, comparable to other state-of-the-art algorithms. Future work includes using more models for the multi-modality strategy, the exploration of algorithms for model selection and centerline fusion.

Acknowledgement

This work was partially supported by Science and Technology Commission of Shanghai Municipality (17JC1401600).

References

[1] National Center for Health Statistic, Mortality Multiple Cause Micro-data Files, 2014: Public-Use Data File and Documentation: Nhlbi Tabulations, (2016) , Accessed date: 15 July 2016.
[2] M. Schaap, C.T. Metz, T.V. Walsum, A.G.V.D. Giessen, A.C. Weustink, N.R. Mollet, C. Bauer, H. Bogunovi, C. Castro, D. Xiang, Standardized evaluation methodology and reference database for evaluating coronary artery centerline extraction algorithms, Med. Image Anal. 13 (5) (2009) 701–714.
[3] H.A. Marquering, J. Dijkstra, P.J.H.D. Koning, B.C. Stoel, J.H.C. Reiber, Towards quantitative analysis of coronary cta, Int. J. Cardiovasc. Imaging 21 (1) (2005) 73–84.
[4] A.F. Frangi, W.J. Niessen, K.L. Vincken, M.A. Viergever, "Multiscale Vessel Enhancement Filtering," *Medical Image Computing and Computer-Assisted Interventation MICCAI98*, (1998), pp. 130–137.
[5] G. Yang, P. Kitslaar, M. Frenay, A. Broersen, M.J. Boogers, J.J. Bax, J.H.C. Reiber, J. Dijkstra, Automatic centerline extraction of coronary arteries in coronary computed tomographic angiography, Int. J. Cardiovasc. Imaging 28 (4) (2012) 921–933.
[6] C. Bauer, H. Bischof, Edge based tube detection for coronary artery centerline extraction, The Midas Journal, 2008 MICCAI Workshop – Grand Challenge Coronary Artery Tracking, 2008 http://hdl.handle.net/10380/1403.
[7] B. Lam, Y. Shu, Y. Hong, A novel vessel segmentation algorithm for pathological retina images based on the divergence of vector fields, IEEE Trans. Med. Imaging 27 (2) (2008) 237–246.
[8] L. Risser, F. Plouraboue, X. Descombes, Gap filling of 3-d microvascular networks by tensor voting, IEEE Trans. Med. Imaging 27 (5) (2008) 674–687.
[9] S. Cetin, A. Demir, A. Yezzi, M. Degertekin, G. Unal, Vessel tractography using an intensity based tensor model with branch detection, IEEE Trans. Med. Imaging 32 (2) (2013) 348–363.
[10] R. Moreno, S. Orjan, Gradient-based enhancement of tubular structures in medical images, Med. Image Anal. 267 (1) (2015) 19–29.
[11] M.W. Law, A.C. Chung, Efficient implementation for spherical flux computation and its application to vascular segmentation, IEEE Trans. Image Process. A Publ. IEEE Signal Process. Soc. 18 (3) (2009) 596–612.
[12] D. Lesage, E.D. Angelini, I. Bloch, G. Funka-Lea, Bayesian maximal paths for coronary artery segmentation from 3d ct angiograms, International Conference on Medical Image Computing and Computer-Assisted Intervention, 2009, p. 222.
[13] M.A. Gülsün, G. Funka-Lea, P. Sharma, S. Rapaka, Y. Zheng, Coronary centerline extraction via optimal flow paths and cnn path pruning, International Conference on Medical Image Computing and Computer-Assisted Intervention, 2016, pp. 317–325.
[14] C. Metz, M. Schaap, A. Van der Giessen, T. Van Walsum, Semi-automatic coronary artery centerline extraction in computed tomography angiography data, IEEE International Symposium on Biomedical Imaging: From Nano To Macro, 2007, pp. 856–859.
[15] Y. Zheng, H. Tek, G. Funka-Lea, Robust and accurate coronary artery centerline extraction in cta by combining model-driven and data-driven approaches, International Conference on Medical Image Computing and Computer-Assisted Intervention, 2013, pp. 74–81.
[16] L.M. Lorigo, O.D. Faugeras, W.E.L. Grimson, R. Keriven, R. Kikinis, A. Nabavi, C.F. Westin, Curves: curve evolution for vessel segmentation, Med. Image Anal. 5 (3) (2001) 195–206.
[17] J. Mille, L.D. Cohen, Region-based 2d deformable generalized cylinder for narrow structures segmentation, European Conference on Computer Vision, 2008, pp. 392–404.
[18] K. Haris, S.N. Efstratiadis, N. Maglaveras, C. Pappas, J. Gourassas, G. Louridas, Model-based morphological segmentation and labeling of coronary angiograms, Med. Imaging IEEE Trans. 18 (10) (1999) 1003–1015.
[19] M. Schaap, I. Smal, C. Metz, T.V. Walsum, W. Niessen, Bayesian tracking of elongated structures in 3d images, International Conference on Information Processing in Medical Imaging, 2007, p. 74.
[20] W.C.K. Wong, A.C.S. Chung, Probabilistic vessel axis tracing and its application to vessel segmentation with stream surfaces and minimum cost paths, Med. Image Anal. 11 (6) (2007) 567–587.
[21] O. Friman, M. Hindennach, C. Khnel, H.O. Peitgen, Multiple hypothesis template tracking of small 3d vessel structures, Med. Image Anal. 14 (2) (2010) 160–171.
[22] S. Cetin, G. Unal, A higher-order tensor vessel tractography for segmentation of vascular structures, IEEE Trans. Med. Imaging 34 (10) (2015) 2172–2185.
[23] E. Kerrien, A. Yureidini, J. Dequidt, C. Duriez, R. Anxionnat, S. Cotin, Blood vessel modeling for interactive simulation of interventional neuroradiology procedures, Med. Image Anal. 35 (2017) 685–698.
[24] J.A. Tyrrell, E.D. Tomaso, D. Fuja, R. Tong, K. Kozak, R.K. Jain, B. Roysam, Robust 3-d modeling of vasculature imagery using superellipsoids, IEEE Trans. Med. Imaging 26 (2) (2007) 223–237.
[25] A.F. Frangi, W.J. Niessen, R.M. Hoogeveen, W.T. Van, M.A. Viergever, Model-based quantitation of 3-d magnetic resonance angiographic images, IEEE Trans. Med. Imaging 18 (10) (1999) 946–956.
[26] C. Wang, O. Smedby, An automatic seeding method for coronary artery segmentation and skeletonization in cta, Insight J. (2008).
[27] D. Lesage, E.D. Angelini, I. Bloch, G. Funka-Lea, A review of 3d vessel lumen segmentation techniques: models, features and extraction schemes, Med. Image Anal. 13 (6) (2009) 819.
[28] H. Li, A. Yezzi, Vessels as 4d curves: global minimal 4d paths to extract 3d tubular surfaces, Conference on Computer Vision and Pattern Recognition Workshop, vol. 26, 2007 82–82.
[29] C.T. Metz, M. Schaap, A.C. Weustink, N.R. Mollet, W.T. Van, W.J. Niessen, Coronary centerline extraction from ct coronary angiography images using a minimum cost path approach, Med. Phys. 36 (12) (2009) 5568–5579.
[30] H. Tang, T.V. Walsum, R.S.V. Onkelen, R. Hameeteman, S. Klein, M. Schaap, F.L. Tori, Q.J.A.V.D. Bouwhuijsen, J.C.M. Witteman, A.V.D. Lugt, Semiautomatic carotid lumen segmentation for quantification of lumen geometry in multispectral mri, Med. Image Anal. 16 (6) (2012) 1202–1215.
[31] O. Wink, W.J. Niessen, M.A. Viergever, Multiscale vessel tracking, IEEE Trans. Med. Imaging 23 (1) (2004) 130–133.
[32] L.D. Cohen, R. Kimmel, Global minimum for active contour models: a minimal path approach, Int. J. Comput. Vis. 24 (1) (1997) 57–78.
[33] K. Krissian, H. Bogunovic, J.M. Pozo, M.C. Villa-Uriol, A. Frangi, Minimally interactive knowledge-based coronary tracking in cta using a minimal cost path, the Midas Journal, 2008 MICCAI Workshop Grand Challenge Coronary Artery Tracking, 2008 [Online]. Available: http://hdl.handle.net/10380/1435.
[34] V. Kaul, A. Yezzi, Y. Tsai, Detecting curves with unknown endpoints and arbitrary topology using minimal paths, IEEE Trans. Pattern Anal. Mach. Intell. 34 (10) (2012).
[35] H. Tek, Automatic coronary tree modeling, Midas J. (2008).
[36] P.H. Kitslaar, J. Dijkstra, B. Stoel, J.H.C. Reiber, M. Frenay, E. Oost, Connected component and morpholgy based extraction of arterial centerlines of the heart, Midas J. (2008).
[37] X. Zhuang, W. Bai, J. Song, S. Zhan, X. Qian, W. Shi, Y. Lian, D. Rueckert, Multi-atlas whole heart segmentation of CT data using conditional entropy for atlas ranking and selection, Med. Phys. 42 (7) (2015) 3822–3833.
[38] X. Zhuang, J. Shen, Multi-scale patch and multi-modality atlases for whole heart segmentation of mri, Med. Image Anal. 31 (2016) 77.
[39] M.W. Jelmer, W. v. H. Robbert, A.V. Max, L. Tim, I. Ivana, Coronary artery centerline extraction in cardiac ct angiography using a cnn-based orientation classifier, Med. Image Anal. 51 (2019) 46–60.
[40] Y. Chen, Y. Zhang, J. Yang, Q. Cao, G. Yang, J. Chen, H. Shu, L. Luo, J.L. Coatrieux, Q. Feng, Curve-like structure extraction using minimal path propagation with backtracking, IEEE Trans. Image Process. A Publ. IEEE Signal Process. Soc. 25 (2) (2015) 988–1003.
[41] L. Liu, W. Shi, D. Rueckert, M. Hu, S. Ourselin, X. Zhuang, Coronary centerline extraction based on ostium detection and model-guided directional minimal path, IEEE International Symposium on Biomedical Imaging, 2014, pp. 133–136.
[42] L. Liu, W. Shi, D. Rueckert, M. Hu, S. Ourselin, X. Zhuang, Model-guided directional minimal path for fully automatic extraction of coronary centerlines from cardiac cta, International Conference on Medical Image Computing and Computer-Assisted Intervention, vol. 16, 2013, pp. 542–549.

[43] T. Jerman, F. Pernus, B. Likar, Z. Spiclin, Enhancement of vascular structures in 3d and 2d angiographic images, IEEE Trans. Med. Imaging 35 (9) (2016) 2107–2118.
[44] X. Zhuang, K.S. Rhode, R.S. Razavi, D.J. Hawkes, S. Ourselin, A registration-based propagation framework for automatic whole heart segmentation of cardiac mri, IEEE Trans. Med. Imaging 29 (9) (2010) 1612–1625.
[45] X. Han, M.S. Hoogeman, P.C. Levendag, L.S. Hibbard, D.N. Teguh, P. Voet, A.C. Cowen, T.K. Wolf, Atlas-based auto-segmentation of head and neck ct images, International Conference on Medical Image Computing and Computer-Assisted Intervention, vol. 5424, 2008, pp. 434–441.
[46] Y. Kitamura, Y. Li, W. Ito, Automatic coronary extraction by supervised detection and shape matching, IEEE International Symposium on Biomedical Imaging, 2012, pp. 234–237.
[47] S. Zambal, J. Hladuvka, A. Kanitsar, K. Buehler, Shape and appearance models for automatic coronary artery tracking, Insight (2008) 1–8.
[48] L.M. Perlmutt, M.E. Jay, D.C. Levin, Variations in the blood supply of the left ventricular apex, Investig. Radiol. 18 (2) (1983) 138.
[49] R. Ilia, G. Rosenshtein, J. Weinstein, C. Cafri, A. Abu-Ful, M. Gueron, Left anterior descending artery length in left and right coronary artery dominance, Coron. Artery Dis. 12 (1) (2001) 77.
[50] T. Jerman, F. Pernus, B. Likar, Z. Spiclin, Enhancement of vascular structures in 3d and 2d angiographic images, IEEE Trans. Med. Imaging 35 (9) (2016) 2107–2118.
[51] R.A. Heckemann, J.V. Hajnal, P. Aljabar, D. Rueckert, A. Hammers, Automatic anatomical brain mri segmentation combining label propagation and decision fusion, Neuroimage 33 (1) (2006) 115–126.
[52] W. Chunliang, S. Orjan, Integrating automatic and interactive methods for coronary artery segmentation: let the pacs workstation think ahead, Int. J. Comput. Assist. Radiol. Surg. 5 (3) (2010) 275.

Dengqiang Jia is a PHD student with the Department of Engineering Mechanics, School of Naval Architecture, Ocean and Civil Engineering, Shanghai Jiao Tong University, China.

Xiahai Zhuang is with the School of Data Science, Fudan University, Shanghai, China. He did his PhD (thesis) in Centre for Medical Image Computing, University College London, with Prof. S Ourselin and Prof. D J Hawkes. Before that, he did his master and bachelor degrees in computer science in Shanghai Jiao Tong University and Tianjin University, respectively. Before joining Fudan, he was an associate professor in Shanghai Jiao Tong University. For more information, please see http://www.sdspeople.fudan.edu.cn/zhuangxiahai/).